

Estimation of average fibre length in short-fibre composites by a two-section method

G. Zak^{b,*}, M. Haberer^a, C.B. Park^a, B. Benhabib^a

^aComputer Integrated Manufacturing Laboratory, Department of Mechanical and Industrial Engineering, University of Toronto, 5 King's College Road, Toronto, Ontario, Canada M5S 3G8

^bDepartment of Mechanical Engineering, Queen's University, McLaughlin Hall, Kingston, Ontario, Canada K7L 3N6

Received 23 March 1999; received in revised form 30 November 1999; accepted 7 March 2000

Abstract

A novel and robust experimental technique is proposed for predicting the average fibre length in layered composites by using data generated from two parallel, closely spaced sections of a specimen. The method estimates the average fibre length on the basis of the ratio of matched fibres appearing in both cross-sections to the total number observed in a single cross-section. The experimental results of the two-section method were verified by using a conventional binder burnout process, in which residual fibres were measured and recorded directly. The direct measurement results confirmed the average fibre length predictions of the two-section fibre matching method. © 2000 Elsevier Science Ltd. All rights reserved.

1. Introduction

Properties of fibre-reinforced composites are largely determined by three factors: fibre content, fibre aspect ratio, and fibre orientation. It is widely reported in the literature that some of the processing steps in the fabrication of short-fibre-reinforced polymeric composites can significantly reduce the fibre length through breakage. Reduction of fibre length decreases the modulus and strength of the composite [1]. For example, Kamal et al. [2] reported a decrease from 0.71 to 0.27 mm in injection moulding of short-fibre thermoplastics. Therefore, one cannot reliably use the observed fibre length prior to compounding for modulus and strength prediction.

The most common method for fibre-length evaluation is the direct measurement of fibre lengths after resin burnout [2–8]. However, as proposed in this paper, estimating the average post-process fibre length indirectly from cross-sectional data collected for fibre-orientation measurements can eliminate this additional lengthy procedure. (Note that such an indirect measurement supplies only the *average* fibre length as opposed to the *distribution* obtainable from direct measurements.) In this context, Zhu et al. [9] proposed to

derive the average fibre length in short-fibre composites by calculating the fraction of fibres whose ends have been intersected by the sectioning plane out of a total number of intersected fibres. However, as pointed out by the paper's authors themselves, this method may produce highly inaccurate estimates. In numerous cases, it is difficult to be certain whether one indeed intersected a fibre end (as characterized by an incomplete ellipse boundary). For example, it is possible that the incomplete ellipse boundary is caused by a piece of fibre chipped away by polishing.

In this paper, a novel, more robust method is proposed for the estimation of the average fibre length which is based on data derived from two consecutive closely-spaced parallel sections of a specimen. The method predicts the average fibre length from the ratio of the number of fibres intersected by both sections to that intersected by only one. Following the description of the method in Sections 2 and 3, an example application of the new method and its verification by direct fibre-length measurements are described in Section 4.

2. Determining the average fibre length from two-section fibre data

The fibre length estimation method proposed in this paper utilizes data derived from two consecutive

* Corresponding author.

E-mail address: zak@me.queensu.ca (G. Zak).

closely-spaced sections of a specimen. The fibre length is estimated from the ratio of the number of fibres intersected by both sections to that intersected by only one section. The above information on the numbers of fibre intersections would typically become available as part of applying a cross-sectional method for fibre-orientation measurement, such as the one described in Zak [10]. However, the data could also be extracted specifically for the purposes of fibre length evaluation.

For a method estimating the average fibre length to produce accurate results, the issue of separating the fines and fragments from the “cylindrical” fibres must be addressed. Since the average is the total length of all fibres divided by the total number of fibres, a large number of fragments, if counted, would skew the average towards zero. The need for the lower fibre-length limit exists in any direct length measurement method (e.g. burn-out method) as well as in the proposed method. In a direct measurement method, the lower limit is established by the ability to identify individual fibres and thus to measure their length. In the proposed two-section method, the lower limit is well established by the ability to identify fibre cross-sections as ellipses (see Section 3). A fibre, in order to produce an elliptical cross-section, must have a cylindrical profile of finite length. Fines and fragments will not have the characteristic elliptical cross-section and thus will not be counted.

This section will first derive the fibre length estimates given an assumption of the uniform fibre length and then will show that accounting for the distribution of fibre lengths does not alter the previously derived expressions. The section concludes with the evaluation of the error sensitivity of the proposed estimation method.

2.1. Uniform fibre length

A well-known relationship in quantitative microscopy [11] gives the probability of a randomly positioned section plane intersecting a particle located in a cubical $L \times L \times L$ sample space as:

$$\text{Prob(plane intersects a particle)} = H/L, \quad (1)$$

where H is the extent of the particle along the section plane normal (or *height* for a horizontal plane). Examining Fig. 1 leads to a conjecture that the corresponding range of possible particle-plane intersections for two parallel section planes, separated by a distance z_t , is $(H - z_t)$, which leads to the intersection probability given by:

$$\begin{aligned} \text{Prob(two planes intersect a particle)} \\ = (H - z_t)/L, H > z_t. \end{aligned} \quad (2)$$

In the case of non-spherical particles, such as cylindrical fibres, H will naturally depend on the fibre's orientation with respect to the section plane, Fig. 2. Let this orientation be defined by two angles (ϕ, θ) , where ϕ is the fibre *misalignment angle* with respect to the section normal and θ is the rotation angle about the section normal, or the *azimuth angle*. Then, the fibre's “height” is given by:

$$H = l \cos \phi + d \sin \phi, \quad (3)$$

where l is the fibre length and d is the fibre diameter.

Let the number of fibres oriented at an angle ϕ and intersected by a single section be denoted by $n^I(\phi)$ and those intersected by two sections be denoted by $n^{II}(\phi)$,

$$n^I(\phi) = N_T p(\phi) H / L$$

and

$$n^{II}(\phi) = N_T p(\phi) (H - z_t) / L, \quad (4)$$

where N_T is the total number of fibres in the specimen, and $p(\phi)$ is the probability of finding fibres oriented at an angle ϕ . Then, for a range of ϕ_1 to ϕ_2 , the number of fibres intersected by one cross-section, N^I , and intersected by both cross-sections, N^{II} , is given by the following integrals:

$$N^I = \int_{\phi_1}^{\phi_2} n^I(\phi) \, d\phi \text{ and } N^{II} = \int_{\phi_1}^{\phi_2} n^{II}(\phi) \, d\phi. \quad (5)$$

Substituting Eq. (4) into Eq. (5) and rearranging:

$$N^I = \frac{N_T}{L} \int_{\phi_1}^{\phi_2} p(\phi) H \, d\phi,$$

and

$$N^{II} = \frac{N_T}{L} \left[\int_{\phi_1}^{\phi_2} p(\phi) H \, d\phi - z_t \int_{\phi_1}^{\phi_2} p(\phi) \, d\phi \right]. \quad (6)$$

Taking the ratio of the two fibre counts and substituting for H from Eq. (3):

$$\begin{aligned} \frac{N^{II}}{N^I} &= 1 - \frac{z_t \int_{\phi_1}^{\phi_2} p(\phi) \, d\phi}{\int_{\phi_1}^{\phi_2} p(\phi) H \, d\phi} \\ &= 1 - \frac{z_t \int_{\phi_1}^{\phi_2} p(\phi) \, d\phi}{l \int_{\phi_1}^{\phi_2} p(\phi) \cos(\phi) \, d\phi + d \int_{\phi_1}^{\phi_2} p(\phi) \sin(\phi) \, d\phi} \\ &= 1 - \frac{P z_t}{Q l + R d}, \end{aligned} \quad (7)$$

where $P = \int_{\phi_1}^{\phi_2} p(\phi) \, d\phi$, $Q = \int_{\phi_1}^{\phi_2} p(\phi) \cos(\phi) \, d\phi$ and $R = \int_{\phi_1}^{\phi_2} p(\phi) \sin(\phi) \, d\phi$.

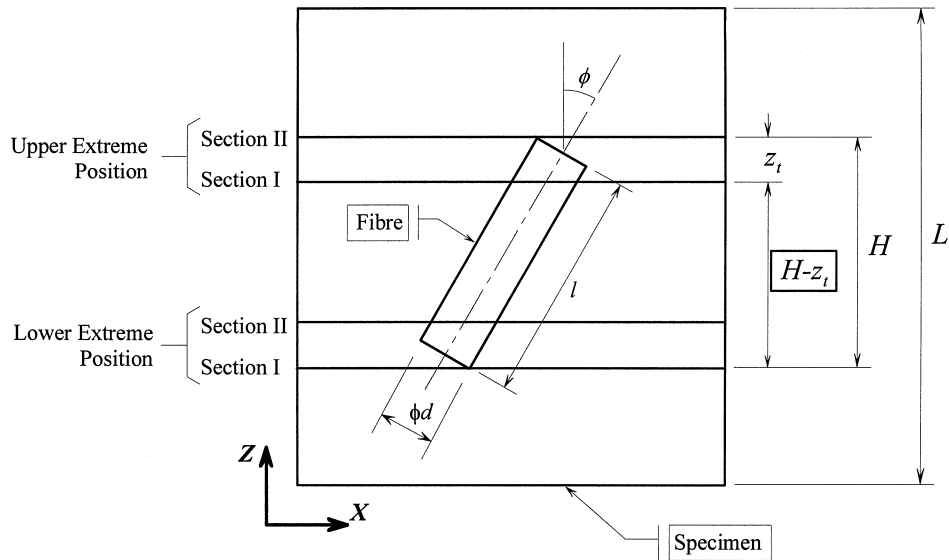


Fig. 1. A pair of section planes shown in upper and lower extreme positions which still lead to the fibre being intersected by both planes.

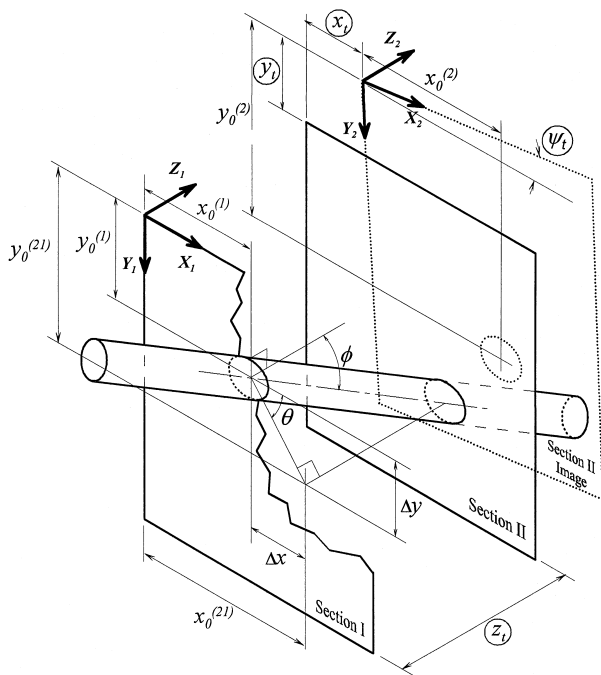


Fig. 2. Geometry of the fibre intersection by two parallel section planes.

Finally, rearranging Eq. (7) one obtains the fibre length as:

$$l = \frac{1}{Q} \left(\frac{Pz_t}{1 - \frac{N^{\text{II}}}{N^{\text{I}}}} - Rd \right). \quad (8)$$

2.2. Fibre-length distribution

Typically, fibre lengths in a short-fibre composite would be characterized by a distribution. In order to represent such a distribution, let us assume that the specimen contains N_i fibres of a discrete length l_i , where the total number of fibres is then defined as:

$$N_T = \sum_{i=1}^m N_i. \quad (9)$$

Considering each subset of N_i fibres of length l_i independently, one can rewrite Eq. (6) as:

$$N_i^{\text{I}} = \frac{N_i}{L} \int_{\phi_1}^{\phi_2} p(\phi)H \, d\phi, \quad (10)$$

and

$$N_i^{\text{II}} = \frac{N_i}{L} \left[\int_{\phi_1}^{\phi_2} p(\phi)H \, d\phi - z_t \int_{\phi_1}^{\phi_2} p(\phi) \, d\phi \right].$$

Substituting for H given in Eq. (3) and using the definitions of the terms P , Q , and R given in Eq. (7), and furthermore by assuming that fibre orientation is independent of fibre length, the above expressions are rewritten as:

$$N_i^{\text{I}} = \frac{N_i}{L} (Ql_i + Rd), \quad (11)$$

and

$$N_i^{\text{II}} = \frac{N_i}{L} (Ql_i + Rd - Pz_t).$$

In order to obtain the number of fibres of all lengths intersected by one and by two sections, the contributions of each length are summed as:

$$N^I = \sum_{i=1}^m N_i^I = \frac{1}{L} \left(Q \sum_{i=1}^m N_i l_i + Rd \sum_{i=1}^m N_i \right),$$

and

$$N^{II} = \sum_{i=1}^m N_i^{II} = \frac{1}{L} \left(Q \sum_{i=1}^m N_i l_i + Rd \sum_{i=1}^m N_i - Pz_t \sum_{i=1}^m N_i \right). \tag{12}$$

The fibre-count ratio can now be written as:

$$\frac{N^{II}}{N^I} = 1 - \frac{Pz_t N_T}{Q \sum_{i=1}^m N_i l_i + R; dN_T} = 1 - \frac{Pz_t}{Q\bar{l} + Rd}, \tag{13}$$

where the average fibre length is defined as:

$$\bar{l} = \frac{\sum_{i=1}^m N_i l_i}{N_T}. \tag{14}$$

Eq. (13) can be rearranged to yield the average fibre length as:

$$\bar{l} = \frac{1}{Q} \left(\frac{Pz_t}{1 - \frac{N^{II}}{N^I}} - Rd \right). \tag{15}$$

Eq. (15) above is equivalent to Eq. (8), which was derived without considering a fibre-length distribution within a specimen. Therefore, the proposed two-section-based fibre-length estimate in Eq. (8) indeed represents the average fibre length.

2.3. Error sensitivity

It would be beneficial to evaluate the robustness of the fibre-length estimate in Eq. (8). Herein, it is assumed that the most significant error sources are the estimates of N^I and N^{II} and thus, the ratio N^{II}/N^I , and the section separation distance z_t .

In Eq. (8), the impact of errors in the term (Rd) can be ignored, as its contribution to the estimate of l is much smaller than the first term's. Evaluating partial derivatives with respect to (N^{II}/N^I) and z_t , the following error estimate is obtained:

$$\Delta l = \left[\left(\frac{-Pz_t}{Q(1-w)^2} \Delta w \right)^2 + \left(\frac{P}{Q(1-w)} \Delta z_t \right)^2 \right]^{1/2}, \tag{16}$$

where $w = N^{II}/N^I$ and Δw and Δz_t are errors in w and z_t , respectively.

The contributions of individual terms and the total error estimate are displayed in Fig. 3 for typical data ($z_t = 13.8 \mu\text{m}$, $w = 0.82$, $P = 0.52$, $Q = 0.5$, $R = 0.134$, yielding $l = 76.4 \mu\text{m}$). The plot shows that the fibre length estimate is highly sensitive to the error in the ratio w : namely, a potential error of about 2–3% in w would result in 10–15% variability in the length estimate. On the other hand, contribution of the z_t error is relatively insignificant.

3. Matching fibre ellipses between cross-sections

Practical application of the theoretical expressions formulated in the preceding section requires that, for each fibre intersecting either of the section planes, it is known whether the fibre passes through *both* planes or only through either one of them. To obtain such information, one would need to identify for each elliptical fibre cross-section on one section plane whether there exists a *matching fibre cross-section* on the other plane which belongs to the same fibre. Our experience of analyzing cross-sectional images of short-fibre specimens has shown that this is not a trivial task. Several specific problems contributing to the task's difficulty have been identified.

The first problem arises because, after examining the first section and prior to examining the second section, the specimen must be removed from the set-up for repolishing. This step may yield an undesirable (and unknown) relative translation and rotation between the images of the two sections.

The second problem is caused by the variability of fibre orientations within the short-fibre composite. When a fibre is intersected by two offset parallel planes,

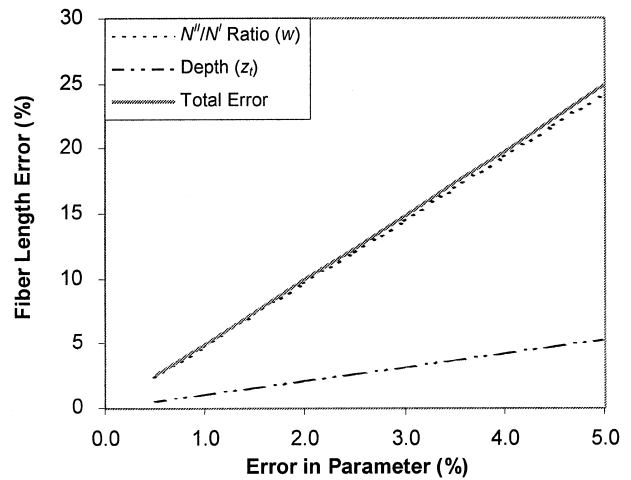


Fig. 3. Error sensitivity of the average length estimate based on the two-section data.

the location of the elliptical cross-section within the second section plane shifts relative to the coordinate frame fixed to the first section by $(\Delta x, \Delta y)$, Fig. 2. This shift is naturally a function of the fibre's orientation, (ϕ, θ) , and, therefore, varies from fibre to fibre.

The third problem is caused by the short length of the fibres considered herein. For such short fibres, a significant fraction will not extend from one section to another, and, therefore, there will not be two matching cross-sections.

Due to the above problems, the pattern of fibre cross-sections changes significantly from one section to the other, which makes it impossible to reliably identify the matching fibres based on the raw cross-sectional images. Therefore, a method has been developed to assist with fibre matching process by predicting the locations of the Section II fibre ellipses based on the fibre ellipse data from Section I. The steps involved in fibre matching are:

1. Identify all the fibre ellipse boundaries in Sections I and II, (Section 3.1);
2. Obtain fibre orientations based on the fibre ellipses in Section I, (Section 3.1);
3. Predict locations of fibre ellipses in Section II based on (a) the fibre orientations derived from Section I ellipses and (b) an approximate estimate of the distance between section planes, \bar{z}_i , (Section 3.3);
4. Translate and rotate fibre ellipses observed in Section II in order to express them in Section I coordinates. Use approximate estimates of parameters (\bar{x}_i, \bar{y}_i) for translation and ψ_i for rotation, (Section 3.3);
5. Superimpose the predicted locations of Section I fibre ellipses over the Section II ellipses (all expressed with respect to the Section I frame), (Section 3.3);
6. Switch each fibre's orientation as needed between the two possible alternatives of the ellipse-based orientation estimate, with the consequent difference in the shift direction, (Section 3.4); and,
7. Identify the ellipses closest in terms of location, shape, and orientation as "matching" (i.e. belonging to the same fibre).

3.1. Estimating fibre orientation

As noted in Steps (1) and (2) above, fibre orientation must be calculated from a single cross section as part of the matching process. Bay and Tucker [12], Fischer and Eyerer [13], Hine et al. [14], and Zhu et al. [9] all measure short-fibre orientations by examining single polished cross-sections with an optical microscope. Their method considers the intersection of a cylinder (i.e. a fibre) with a plane, to calculate the misalignment

angle ϕ between the plane's normal and the cylinder's longitudinal axis:

$$\phi = \arccos(B/A), \quad (17)$$

where A is the major radius and B is the minor radius of the ellipse, respectively. The azimuth angle, θ , is defined by the direction of the major axis.

3.2. Estimating section-to-section transformation parameters

Step (4) of the fibre matching procedure requires values of four section-to-section transformation parameters: x_i, y_i, z_i , and ψ_i , (these parameters are circled in Fig. 2). The (x_i, y_i) pair represents the in-plane shift between the images of the two sections; z_i is the separation distance between the section planes; and ψ_i is the rotation angle about Z-axis which aligns the two section frames. It is assumed that the ψ_i angle is small and that the section planes are parallel to each other.

First, it must be noted that, since the matching process only requires making the binary "match" vs. "no-match" decisions, the parameter values do not need to be precisely known at this stage. Additionally, an approximate value for z_i should be available because the thickness of material removed would be usually monitored during the repolishing step.

Second, one can use specimen features which extend through both planes and are perpendicular to the planes to approximately estimate the in-plane shift. These features may be the specimen edges or fibres nearly aligned with the section-plane normal.

The parameter estimates can then be further refined through an iterative process. Once a minimal number of matching fibres has been identified, a more accurate estimate of the transformation parameters can be made using a methodology developed for evaluating fibre orientation in Zak [10]. These estimates can in turn be used to enhance the accuracy of the ellipse overlapping display. As more fibres are matched, the accuracy of the parameter estimates would be further improved.

3.3. Superimposing the fibre ellipses

For the ellipses to be matched, they must be superimposed on the same display. To accomplish this task, the predicted locations of Section I fibre ellipses are superimposed over the Section II ellipses expressed with respect to the Section I frame. Before giving the expressions for the locations of the superimposed ellipses, several definitions are introduced below.

First, let the centre coordinates of a Section I ellipse be $(x_o^{(1)}, y_o^{(1)})$ and those of a Section II ellipse be $(x_o^{(2)}, y_o^{(2)})$, Fig. 2. These are the locations of the ellipse centres in the respective coordinate frames of each section. They

are obtained, for example, by examining the images of the specimen cross-sections.

Next, let $(\hat{x}_o^{(21)}, \hat{y}_o^{(21)})$ be the projected location of a Section I ellipse centre, $(x_o^{(1)}, y_o^{(1)})$, along the fibre's longitudinal axis at the depth of Section II, but expressed in Section I frame, and let $(x_o^{(21)}, y_o^{(21)})$ be the centre of the Section II ellipse, $(x_o^{(2)}, y_o^{(2)})$, transformed to the Section I frame.

For the Section I ellipses, the projection is made based on the fibre's orientation (ϕ, θ) obtained as described in Section 0 above:

$$\hat{x}_o^{(21)} = x_o^{(1)} + \tilde{z}_t \tan \phi \cos \theta^*$$

and

$$\hat{y}_o^{(21)} = y_o^{(1)} + \tilde{z}_t \tan \phi \sin \theta^*, \quad (18)$$

where the azimuth angle $\theta^* = \theta$ or $\theta^* = \theta + \pi$, depending on which of the two alternative orientations is selected; ϕ is estimated using Eq. (17) and \tilde{z}_t is the initial approximate estimate of the parameter z_t .

In order to express the centres of Section II ellipses in the Section I frame, they are first rotated by angle ψ_t and then translated by $(\tilde{x}_t, \tilde{y}_t)$:

$$x_o^{(21)} = x_o^{(2)} \sin \psi_t - y_o^{(2)} \cos \psi_t + \tilde{x}_t$$

and

$$y_o^{(21)} = x_o^{(2)} \cos \psi_t + y_o^{(2)} \sin \psi_t + \tilde{y}_t, \quad (19)$$

where $(\tilde{x}_t, \tilde{y}_t)$ are the initial estimates of the parameters (x_t, y_t) .

The transformed ellipses from both sections can now be matched by displaying them simultaneously. After the correct orientation alternative for the projected Section I ellipses has been selected, as described in the following subsection, the two displays should ideally overlap.

3.4. Selecting correct orientation alternative

Projecting Section I ellipses at the Section II depth requires selection of the correct alternative from the two possible orientations ($\theta^* = \theta$ or $\theta^* = \theta + \pi$). The correct orientation is found by examining each of the two alternatives and selecting the one which produces a closer match. In the current implementation, this step is performed manually, whereby a Section I ellipse is "toggled" between the two alternatives through operator's action and the closer match is visually identified. Then, the ellipses are matched and the fibre's orientation alternative is recorded together with the identifications of the matching ellipses.

The above process is expected to be well-suited for automation, since the matching decisions can be made

by automatically toggling between the alternative orientations and seeking the closest matches in terms of ellipse orientation, eccentricity, and minor diameter.

4. Average fibre-length estimation from cross-sectional images

4.1. Experimental procedure

Collection of fibre-orientation and fibre-length data is a time-consuming task, with the bulk of the time spent on the manual acquisition of the fibre cross-section boundary data from digitized images. Given below are the primary steps required to collect the raw data and to derive the fibre orientations and the average fibre length:

1. set specimens in a resin mould;
2. mill the top surface of the mould to obtain a uniform planar surface;
3. polish the surface of the mould encasing the specimen;
4. acquire digitized images of the desired cross-section region;
5. collect fibre ellipse cross-section data.

Repeat Steps 3–5 for two closely-spaced (10–15 μm in our case) consecutive cross sections;

6. identify matching fibre ellipses in Sections I and II;
7. calculate the average fibre length.

4.1.1. Specimen description

Fibre orientations and average fibre lengths were calculated for a sample of four specimens selected from a larger set of *layered* composite specimens. Each specimen consisted of 13 layers, each layer nominally 0.3 mm thick. The layered composites contained 18% of Owens Corning 737BD 1/16" milled glass fibres in a matrix of UV-cured Cibatool SL5170 photopolymer. Table 1 lists the measured volumetric fibre content for the four specimens.

4.1.2. Image acquisition

Due to the time-consuming nature of the fibre-orientation measurements, only several layers within each of

Table 1
Fibre content by volume

Specimen name	Fibre content (%)
No. 1	16.4
No. 2	17.9
No. 3	16.9
No. 4	14.7

the four specimens were examined. The specimens were examined via a microscope (Olympus Vanox) under a yellow-filtered reflected light. Images were acquired using a CCD video camera (Sony XC-77) passing its signal to a frame grabber (Scion LG3) at a resolution of 640×480 pixels, with 256 grey levels per pixel. Each image captured an area of $0.5 \times 0.4 \text{ mm}^2$, translating to a spatial resolution of $0.83 \mu\text{m}$ per pixel.

4.1.3. Matching fibres between sections

Once the combined data for both consecutive specimen sections is obtained, ellipses belonging to the same fibres must be identified. To facilitate the fibre-matching task, custom software was written in MATLAB[®]. The developed software overlays ellipse outlines from both sections onto the same display, as described in Section 3 of this paper. Fig. 4 shows an example of a Section II image; Fig. 5 displays the ellipse boundaries extracted from Section I and II images of the same area; and,

finally, Fig. 6 provides an overlaid display of both section ellipses after necessary transformations.

4.2. Experimental results

Each image required about 25–30 min of processing for collection of ellipse data and a similar time for each image-pair for fibre matching. Including section preparation, image acquisition, and other steps, the experiments took about 150 h. The results of the section-to-section matching are shown in Table 2.

Average fibre lengths were estimated for all the specimens using the methodology described in Section 2. To simplify calculations, the length estimates were made using only fibres with the misalignment angle in the range $0^\circ < \phi < 30^\circ$ (ϕ calculated from single-section orientation data). At low misalignment angles, the effect of the orientation-dependent bias, which reduces the chance of intersection for fibres with increasing misalignment

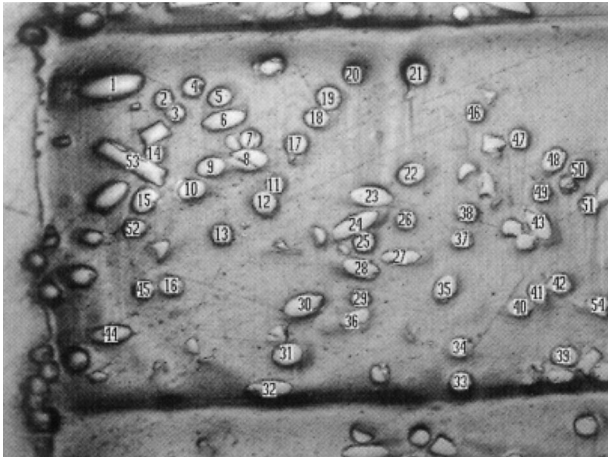


Fig. 4. An example image of a specimen cross-section.

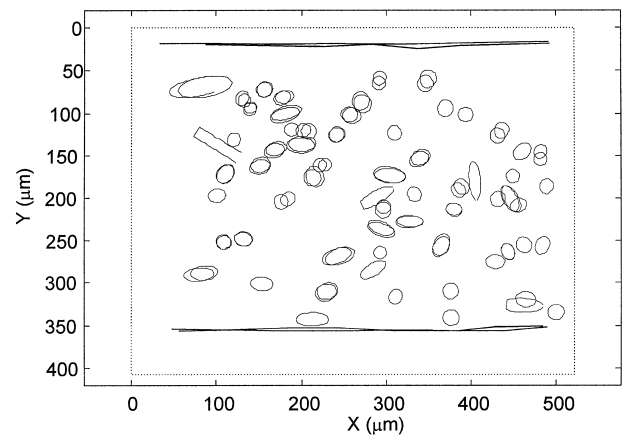


Fig. 6. Overlaid display of fibre ellipses from two sections.

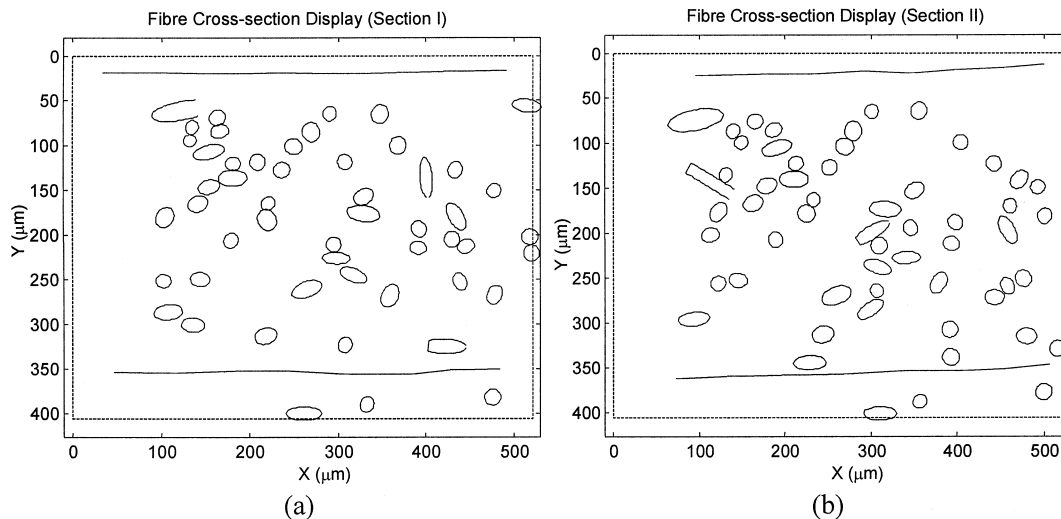


Fig. 5. Fibre ellipses obtained from two consecutive sections, with Section II (b) further into the specimen than Section I (a) by $14 \mu\text{m}$.

angles, is insignificant. Therefore, the effect of fibre orientation on overall length prediction based on the ratio $N^{\text{II}}/N^{\text{I}}$ can be safely ignored. The fibre matching results and $N^{\text{II}}/N^{\text{I}}$ ratios are given in Table 3.

A second simplifying assumption was that the fibres are distributed uniformly within the angular range considered. Thus, $p(\phi) = K$ (K is a constant), $\phi_1 = 0$, and $\phi_2 = \pi/6$, which yields factors P , Q , and R in Eq. (8) as $P = \frac{\pi}{6}K$, $Q = \frac{1}{2}K$, and $R = \left(1 - \frac{\sqrt{3}}{2}\right)K$. For example, using the data for Specimen no. 1 (fibre diameter $d = 16 \mu\text{m}$, section separation depth $z_t = 13.8 \mu\text{m}$, $N^{\text{II}} = 344$, and $N^{\text{I}} = 414$) yields an average fibre length estimate of $84 \mu\text{m}$. All estimation results are given in Table 4.

4.3. Fibre-length measurements via binder burnout

In order to verify the length predictions obtained from section matching data, a reliable, independent experimental technique was utilized. A binder burnout

process was developed based on a thermogravimetric analysis of Cibatool SL5170 resin [15]. The temperature was increased to 300°C , held for 2 h, and then increased to 530°C and held for an additional hour. The recovered fibres were placed in a petri dish and dispersed in alcohol. Photomicrographs were acquired via the same CCD camera and microscope used previously, and the captured images were digitized. In order to reduce the undercounting of long fibres due to the small size of a single image, a matrix of four images was combined by matching fibre ends common to adjacent images (Fig. 7). Three such combined photomicrographs were assembled from random locations within the Petri dish. The digitized images were processed with a custom-written MATLAB[®] based software.

The length of each completely visible fibre was obtained by visually locating both of its ends and then converting the length from pixels to millimetres using the calibration data. Fibre length distributions are generally described by asymmetrical histograms, with short fibres constituting the majority. Therefore, such histograms can be well-represented by the Weibull

Table 2
Results of section-to-section matching

Specimen	Number of matched fibres	Number of fibres used to estimate parameters	x_t (μm)	y_t (μm)	z_t (μm)	ψ_t (deg)
No. 1	647	303	-6.4 ± 1.4	-8.4 ± 0.9	13.9 ± 0.5	1.45
No. 2	928	300	25.9 ± 0.8	8.7 ± 1.6	10.8 ± 0.9	0.45
No. 3	504	195	3.1 ± 0.6	-10.9 ± 0.5	10.0 ± 0.8	0.93
No. 4	120	80	41.7 ± 1.3	7.3 ± 1.8	11.4 ± 0.7	2.1

Table 3
Fibre matching ratios

Specimen	Number of matched fibres, N^{II}	Total number of fibres with $\phi < 30^\circ$, N^{I}	Ratio ($N^{\text{II}}/N^{\text{I}}$)
No. 1	344	414	0.831
No. 2	621	683	0.909
No. 3	313	350	0.894
No. 4	39	48	0.813

Table 4
Fibre length verification results

Specimen	Two-section method	Binder burnout method		
	Predicted average fibre length (μm)	Total number of fibres examined	Estimated mean fibre length (μm)	Estimated standard deviation (μm)
No. 1	84	838	114	88
No. 2	138	1368	113	67
No. 3	110	1516	115	70
No. 4	54	937	101	70

distribution [4,16]. Individual fibre measurements in this paper were thus combined to produce fibre-length histograms, which were fitted to a two-parameter Weibull distribution:

$$p(l) = \frac{b}{a} \left(\frac{l}{a}\right)^{b-1} e^{-\left(\frac{l}{a}\right)^b}, \quad l > 0, \quad (20)$$

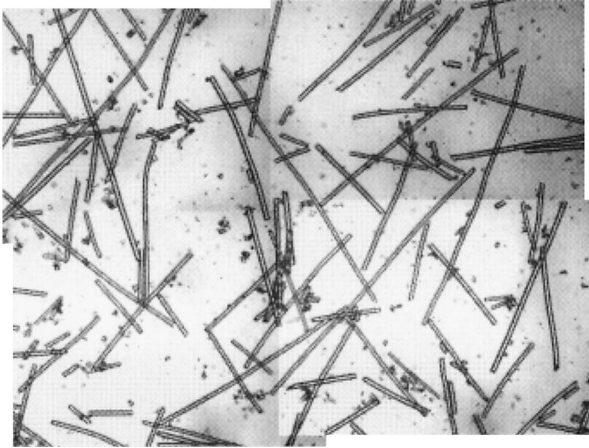


Fig. 7. A combined photomicrograph for Specimen no. 1.

where a and b are shape parameters and l is the fibre length. The two shape parameters were determined by a linear regression fit of the ordered fibre lengths versus a cumulative distribution function plotted on a logarithmic scale [17]. The histogram data and the fitted Weibull plots are displayed in Fig. 8 for all four specimens. The mean lengths and standard deviations were obtained from the fitted Weibull PDF.

Thieltges and Michaeli [8], who employ a fibre measurement scheme similar to that outlined above, state that, in order to gain statistically significant results, it is necessary to measure over 500 individual fibres from each sample, with over 800 fibres recommended. Thus, in order to assure the reliability of the estimations, the smallest sample comprised 838 fibres (Specimen no. 1), Table 4.

From Table 4, the combined weighted average of the mean fibre lengths for the four specimens is 111 μm , with a variance of only $\pm 5 \mu\text{m}$ between specimens. In comparison, the combined weighted average of the lengths predicted by the two-section method is 114 μm , with a variance of $\pm 25 \mu\text{m}$. Thus, the average length predicted by the two-section method proposed in this paper is within 3% of the mean fibre length obtained by direct measurements. Comparing the two methods

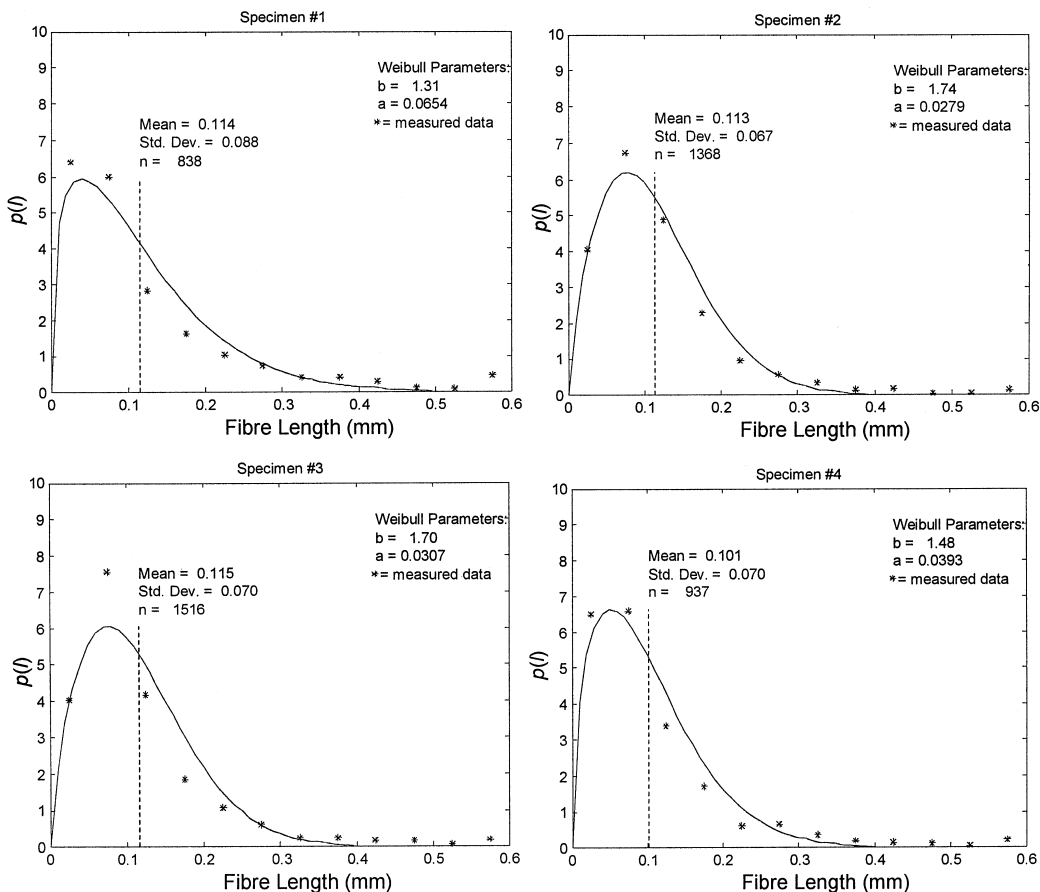


Fig. 8. Weibull plots of fibre-length distributions.

specimen by specimen, all the average fibre lengths predicted by the two-section method are well within one standard deviation of the estimated population mean found through the binder-burnout process. Thus, one can conclude that the two-section method proposed in this paper is capable of providing accurate predictions of the average fibre length.

5. Conclusions

In this paper, a novel method is proposed for estimating the average fibre length in short-fibre reinforced composites. This technique estimates the fibre length by calculating the ratio between the number of fibres intersected by two consecutive, closely spaced sections and the number intersected by a single section plane. The estimates were verified independently through a conventional procedure involving binder burnout and direct measurement of fibre lengths in the residue. It was found that the average fibre length predicted by the two-section method is in good agreement with the average length obtained through the binder burnout.

Acknowledgements

We gratefully acknowledge the financial support of the Natural Sciences and Engineering Research Council of Canada and would like to thank Professor M.R. Piggott for providing access to metallographic polishing facilities and image acquisition equipment.

References

- [1] Piggott MR. Load-bearing fibre composites. New York: Pergamon Press, 1981.
- [2] Kamal MR, Song L, Singh P. Measurement of fibre and matrix orientations in fibre reinforced composites. *Polymer Composites* 1986;7(5):323–9.
- [3] Arroyo M, Avalos F. Polypropylene/low density polyethylene blend matrices and short glass fibers based composites. I mechanical degradation of fibers as a function of processing method. *Polymer Composites* 1989;10(2):117–21.
- [4] Chin W, Liu H, Lee Y. Effects of fiber length and orientation distribution on the elastic modulus of short fiber reinforced thermoplastics. *Polymer Composites* 1988;9(1):27–35.
- [5] Eriksson PA, Albertsson AC, Boydell P, Prautzsch G, Manson JA. Prediction of mechanical properties of recycled fiberglass reinforced polyamide 66. *Polymer Composites* 1996;17(6):830–9.
- [6] Franzen B, Klason C, Kubat J, Kitano T. Fiber degradation during processing of short fiber reinforced thermoplastics. *Composites* 1989;20(1):65–76.
- [7] Gupta VB, Mittal RK, Sharma PK, Menning G, Wolters J. Some studies on glass fiber-reinforced polypropylene. part I: reduction in fiber length during processing. *Polymer Composites* 1989;10(1):8–15.
- [8] Thielges HP, Michaeli W. Effects on fiber length during processing. *SPE ANTEC Technical Papers* 1991;37:1991–3.
- [9] Zhu RT, Blumenthal WR, Lowe TC. Determination of non-symmetric 3-D fiber-orientation distribution and average fiber length in short-fiber composites. *Journal of Composite Materials* 1997;31(13):1287–302.
- [10] Zak G. Rapid layered manufacturing of short-fibre-reinforced parts. PhD thesis, University of Toronto: Department of Mechanical and Industrial Engineering, 1998.
- [11] DeHoff RT, Rhines FN. Quantitative microscopy. New York: McGraw-Hill, 1968 (pp. 129–131).
- [12] Bay RS, Tucker III CL. Stereological measurement and error estimates for three-dimensional fibre orientation. *Polymer Engineering and Science* 1992;32(4):240–53.
- [13] Fischer G, Eyerer P. Measuring spatial orientation of short fibre reinforced thermoplastics by image analysis. *Polymer Composites* 1988;9(4):297–304.
- [14] Hine PJ, Duckett RA, Davidson N, Clarke AR. Modelling of the elastic properties of fibre reinforced composites. I: orientation measurements, *Composites Science and Technology* 1993;47:65–73.
- [15] Liao H. Stereolithography using compositions containing ceramic powders. PhD thesis, University of Toronto: Department of Metallurgy and Materials Science, 1997.
- [16] Fu S-Y, Lauke B. Effects of fibre length and fibre orientation distributions on the tensile strength of short-fibre-reinforced polymers. *Composites Science and Technology* 1996;56:1179–90.
- [17] Kennedy JB, Adam MN. Basic statistical methods for engineers and scientists. New York: Harper and Row, 1986 (pp. 248–253).